Can turbulence explain the formation of void regions in clouds?

Javier Sierra-Ausin,[1] Alain Pumir,[1] Mohsen Bagheri,[2,3] Kim Ye Won,[2,3]
Eberhard Bodenschatz,[2,3] Bernard Mehlig,[4] and Kristan Gustavsson[4]

[1] *Laboratoire de Physique, ENS de Lyon, Université de Lyon 1 and CNRS, 69007 Lyon, France*
[2] *Max Planck Institute for Dynamics and Self-Organization, 37077 Göttingen, Germany*
[3] *Institute for the Dynamics of Complex Systems, University of Göttingen, Friedrich-Hund-Platz 1, Göttingen, D-37077 Germany*
[4] *Department of Physics, Gothenburg University, Gothenburg, SE-40530 Sweden*

(Dated: January 11, 2026)

Fluid particles transported by incompressible turbulent flows become uniformly distributed in space. In contrast, inertial particles can be unevenly distributed in the flow. Although in clouds, small droplets have a very small inertia, we observe the presence of voids, i.e. small regions where droplets are essentially absent. This is consistent with the results of numerical simulations, which reveal the presence of voids even when the inertia of the particles is very small.We explain this unexpected manifestation of fluid inertia by the effect of vortices of moderate intensity, which are sufficiently persistent in time to expel droplets. Our results explain the extreme sensitivity of void formation on the inertia of particles.

Dust particles in circumstellar accretion disks [1], respiratory droplets in exhaled air [2], or small water droplets in atmospheric clouds [3–5] are transported by a turbulent fluid, although their weak inertia prevents them from following exactly the flow. In incompressible turbulent flows, tracer particles, in the absence of any inertial effects follow the flow, and their spatial distribution must remain or become homogeneous. A remarkable effect of particle inertia is that it could lead to inhomogeneous spatial distribution, even if the flow is incompressible [6]: particles heavier than the fluid are centrifuged out of vortical regions in the turbulent fluid. This could lead to the accumulation of particles in certain regions of the flow, which may in turn facilitate collisions, a process that favors the formation of rain drops by aggregation of smaller droplets [4, 7, 8]. In practice, however, the weakness of the droplet inertia makes it questionable whether this effect could be play any role in for cloud microphysics [9]. However, recent experiments in cloudy conditions have shown the sporadic appearance of voids in clouds [10], and recent measurements in clouds also provided evidence for weak clustering of small droplets [11, 12].

In a cloud physics context, it has been extensively documented that entrainment and mixing of dry air from air outside the cloud can generate substantial inhomogeneities in the droplet distribution inside the cloud [13], therefore providing a potential explanation for the observation of voids. More recently, numerical simulations of suspensions of particles with low inertia have shown the existence of void regions in the flow in an otherwise completely homogeneous suspension [14, 15].

The ambiguous understanding of the inertial effects of small particles largely stems from the lack of high-resolution *in-situ*data needed to resolve cloud microphysics [5, 9] and from the limited attention given to low-Stokes-number particles ($\mathrm{St} < 0.1$) in both experimental [16–19] and numerical [20–22] studies. Recent advances in high-resolution airborne *in-situ* measurement systems, however, now allow direct characterization of cloud microphysics in real atmospheric conditions, including the behavior of low-Stokes-number particles.

Here, we ask whether the effects of inertia could be the reason for the formation of voids in clouds. To this end, we used *in-situ* measurements of cloud droplets in turbulent clouds, giving access to particle sizes and to the properties of turbulence. Figure 1 shows representative *in situ* PIV images from the EUREC^{4}A campaign [23] at increasing Stokes numbers. Void regions are frequently observed within the cloud, particularly at larger Stokes numbers.

Our observations indicate that small cloud droplets, of radius of the order $5 - 20\mu$m, with a very inertia (quantified by small Stokes numbers $\mathrm{St} \sim 10^{-2}$) can exhibit inhomogeneous spatial distributions, and that the presence of these inhomogeneities strongly depends on the Stokes number itself. The sizes of these regions can be as large as $\sim$ 2cm, which corresponds to approximately $\sim 30\eta$, where η is the Kolmogorov size, i.e. the size of the smallest eddies in the flow.

Numerically, we observe that voids can also form in a suspension of weakly inertial particles in a direct numerical simulation (DNS) of turbulent flow. In fact, we demonstrate that the statistics of voids obtained from the field campaign and from DNS, as measured by the probability density function (PDF) of Voronoi sizes [18], agree very well. Further analysis of the numerical results allow us to explain the formation of voids by a cumulative expulsion of weakly inertial particles by regions of strong vorticity. Interestingly, we demonstrate that the mechanism leading to the expulsion observed in clouds is not due to the most intense vortices, which are too rare, but rather to vortices of intermediate strength, which are persistent enough in time to empty regions of size $\sim 30\eta$. Our analysis also explain the sensitivity of the void forma-

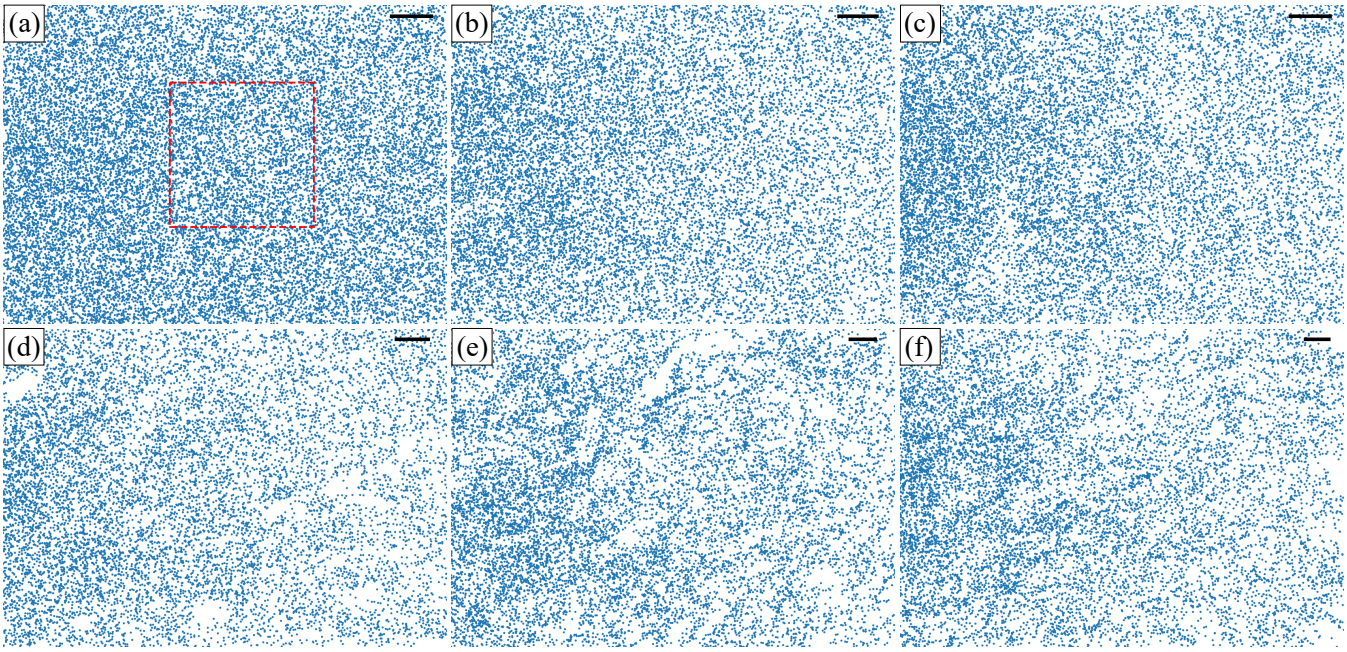

FIG. 1: Representative particle images with an increase in the Stokes number observed during the EUREC^{4}A campaign. ⟨St⟩: (a) 0.013 (0.97), (b) 0.025 (1.00), (c) 0.035 (1.03), (d) 0.045 (1.04), (e) 0.056 (1.11), (f) 0.085 (1.27). $\langle St \rangle$ is a time-averaged Stokes number; each image corresponds to the frame with median value of a each St range. Values in parentheses are inhomogeneity indices from the Voronoi cell area distribution (see Figure 3). The Stokes number and Voronoi cell area are calculated based on the square region shown in the (a) with red dashed lines. The physical scale of the image is $13.6 \times 9.8\ cm^2$. The images were generated from the particle positions, each represented with a radius of 0.3 mm, and a scale bar corresponding to 15η is provided.

tion process on particle inertia, measured by the Stokes number.

In our study, we consider the motion of small particles or radius a, located at a position $\mathbf{x}_p$ and moving with a velocity $\mathbf{v}$ in a turbulent fluid, with velocity $\mathbf{u}$ at the location of the particles. In the limit of very small particle Reynolds number, $\mathrm{Re}_p = |\mathbf{u} - \mathbf{v}|a/\nu \ll 1$, the equations of motion reduce to:

$$\frac{d\mathbf{v}}{dt} = \frac{1}{\tau_p}(\mathbf{u}(\mathbf{x}_p) - \mathbf{v}) \ , \quad \frac{d\mathbf{x}_p}{dt} = \mathbf{v} \, , \tag{1}$$

where $\tau_p = \frac{2}{9}\frac{\rho_p}{\rho_f}\frac{a^2}{\nu}$ is the relaxation time of the particle. In a turbulent flow, the time of the fastest eddies is the Kolmogorov time, $\tau_K = (\nu/\epsilon)^{1/2}$, where ϵ is the rate of turbulent energy dissipation per unit mass of the fluid. The dimensionless ratio $\mathrm{St} = \tau_p/\tau_K$ compares the relaxation time of the particle τ_p and the time of the fastest eddies, and measures the inertia of the particles. In atmospheric flows, the values of St are found to be of the order of ~ 0.01 for realistic values of a and of ϵ [9]. These low values suggest that the velocity of the particle adjusts in a short time to the velocity of the fluid when one considers eddies of amplitude $\sim 1/\tau_K$. However, extremely intense vorticity fluctuations develop in the flow, with magnitudes orders of magnitude larger than the typical fluctuation, an effect which could potentially play a role in generating spatially inhomogeneous particle distributions.

Those observation results give us the idea that despite od the small Stokes number, the Voronoi index increases as the Stokes number. Method to calculate the stokes number [**?**]

Figure 2 presents two examples of *in situ* PIV measurements obtained during cloud-kite observations in the EUREC^{4}A campaign [27]. The two measurements were conducted at similar altitudes (approximately 1 km). Compared to FL12, FL6 exhibits approximately twice the droplet number concentration, consistent with a stronger influence of continental aerosol sources. In contrast, FL12 is characterized by a Stokes number approximately four times larger than that of FL6. Moreover, the Stokes number in FL12 shows substantial fluctuations, including within the cloud-core region where entrainment and mixing are expected to be minimal. These fluctuations are associated with pronounced spatial inhomogeneity in the droplet distribution.

To examine whether this sensitivity to the Stokes number is representative of the full dataset, all available PIV measurements are grouped into six Stokes number bins, as summarized in Table I. Only cloud-core regions, identified by approximately steady particle number density

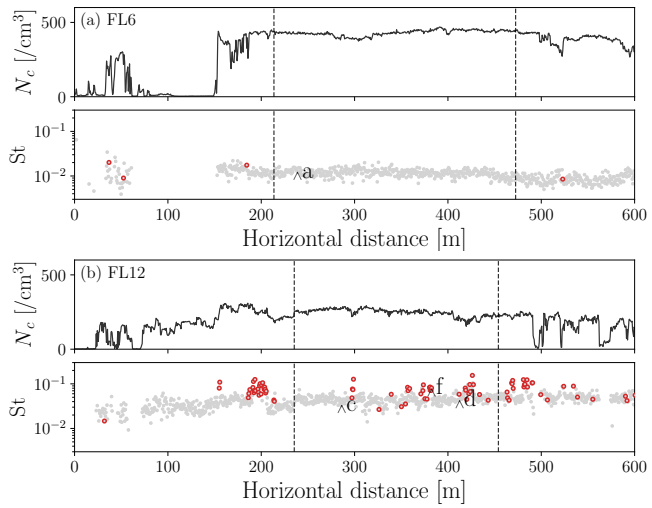

FIG. 2: Particle number concentration (N_c) and St along the horizontal distance of the clouds from EUREC^{4}A campaign. (a) February 4 at 18:43 (FL6), (b)) February 12 at 22:54 (FL12). In the St plot, the red markers denote points corresponding to inhomogeneity indices from the Voronoi cell area distribution larger than 1.

(e.g., indicated by the dashed vertical lines in Fig. 2), are included in the analysis in order to minimize the effects of entrainment and mixing.

, processing curves for each bin.

voids depends mostly on the turbulence from the 4th bins epsilon varies an order of 10 while the mean diameter still remains in same. The Reynolds number not related to the deviation of the right tails in Voronoi area distribution. It is mostly come from the turbulence, not the droplet size, unlikely reported

compare the exp with DNS. The probability density functions of normalized Voronoi cell areas are shown in Figure 3. The distribution obtained for F4 (blue circles) follows a Poisson-Voronoi distribution (shown as black dashed lines). In comparison, the distribution for F12 (red triangles) exhibits heavy tails. The deviation begins at $2.5\,\langle A\rangle$, and corresponds to a probability level of $\sim 10^{-3}$. It reaches a maximum at $\sim 2.8\,\langle A\rangle$ and then decreases until $14.1\langle A\rangle$ which corresponds to 7.5, 8.4, and $42.3\eta^2$, respectively.

The values of St and Sv are small, consistent with Table 1 in [9]. The experiments shown here therefore amply confirm that voids can form in clouds, with droplets of very small inertia, and are also consistent with recent DNS observations [15], and our own simulations, which we will discuss later. The results also point to a sensitivity on St. How to explain these observations, given in particular the remark that the Stokes numbers considered are small, and between St ≈ 0.01 (F4) and St ≈ 0.033 (F12) is the question we consider in turn.

TABLE I: Parameter values for measurements. Dissipation rate per unit mass ε. Droplet diameter d. $\langle\rangle$: time-averaged value. R$_\lambda$ is range between 170 to 2110. The data are collected from nine independent PIV measurements during the EUREC^{4}A campaign, including flights Flight 6 and Flight 12 [**?**], comprising a total of 1740 image sets.

St$_{min}$	St$_{max}$	$\langle$St$\rangle$	$\langle$Sv$\rangle$	$\langle\varepsilon\rangle$ [m^2/s^3]	$\langle R_\lambda\rangle$	$\langle d\rangle$ [μm]
0.005	0.020	0.013	0.253	0.011	1210	12.9
0.020	0.030	0.025	0.374	0.016	1180	16.4
0.030	0.040	0.035	0.399	0.022	1620	17.6
0.040	0.050	0.045	0.446	0.026	1720	19.2
0.050	0.068	0.056	0.414	0.040	1660	19.4
0.070	0.155	0.085	0.325	0.091	1590	19.2

Our analysis is based on the fact that inertia leads to a difference between the velocities of the fluid, $\boldsymbol{v}_{\rm p}$, and of the particles, $\boldsymbol{u}$ [6]. Namely, for small Stokes number St$=\tau_{\rm p}/\tau_{\rm K}\ll 1$, the equation for the dynamics of particles, Eq. (1), can be simply approximated by advection in an effective particle-velocity field [6] $\dot{\boldsymbol{x}}=\boldsymbol{v}_{\rm p}$ with $\boldsymbol{v}_{\rm p}=\boldsymbol{u}-\tau_p{\rm D}\boldsymbol{u}/{\rm D}t$. Effectively, $\boldsymbol{v}_{\rm p}$ differs from $\boldsymbol{u}$ by a quantity proportional to St, and is a compressible field: $\boldsymbol{\nabla}\cdot\boldsymbol{v}_{\rm p}=-\tau_{\rm p}{\rm tr}\mathbb{A}^2=-\tau_{\rm p}({\rm tr}\mathbb{S}^2-{\rm tr}\mathbb{O}^T\mathbb{O})$, where we denote by $\mathbb{A}$ the velocity gradient tensor, and $\mathbb{S}\equiv(\mathbb{A}+\mathbb{A}^T)/2$ and $\mathbb{O}\equiv(\mathbb{A}-\mathbb{A}^T)/2$ its symmetric and antisymmetric components. Inertial droplets tend to avoid sinks of the effective velocity field $\boldsymbol{v}_{\rm p}$ i.e. vortical regions with large values of $\omega=|\boldsymbol{\omega}|$ [6, 28].

The number density $n(\boldsymbol{x}_t,t)$ of droplets advected by $\boldsymbol{v}_{\rm p}$, evolves according to [7, 29]

$$\begin{aligned} n(\boldsymbol{x}_T,T) &= n_0\exp\Big[-\int_{-T}^{0}{\rm d}t'\,\boldsymbol{\nabla}\cdot\boldsymbol{v}_{\rm p}(t')\Big] \\ &= n_0\exp\Big[\mathcal{I}_T(\boldsymbol{x}_0)\Big], \end{aligned} \tag{2}$$

where:

$$\mathcal{I}_T(\boldsymbol{x}_0)={\rm St}\times\tau_K\int_{-T}^{0}{\rm d}t'\,{\rm tr}\mathbb{A}^2(t') \;={\rm St}\times\mathcal{I}'_T(\boldsymbol{x}_0)\,, \tag{3}$$

the integral in Eq. (3) being integrated along a particle trajectory. Having in mind the limit of small St, we focus on tracer particles [7]. For typical fluctuations of the velocity gradient, ${\rm tr}\mathbb{A}^2=({\rm tr}\mathbb{S}^2-\omega^2/2)$ is of order τ_K^{-2}, which suggests that for a duration of order $\sim 10\tau_K$, the integral $\mathcal{I}'_T\lesssim 10$. This estimate implies that the integral $\mathcal{I}_T(\boldsymbol{x}_0)$ remains small, so $n(\mathbf{x}_T,T)$ should remain close to n_0. For this reason, particles with St ~ 0.01 are expected to be almost uniformly distributed [9]. This makes it difficult to understand the origin of the inhomogeneities in the distribution of droplets, clearly seen in Figs. (2,3).

The shortcoming of the argument above is that very strong fluctuations of the velocity gradient tensor appear in the flow [30], carried in particular by very intense vortex tubes, where the values of ${\rm tr}(\mathbb{A}^2)$ are very negative.

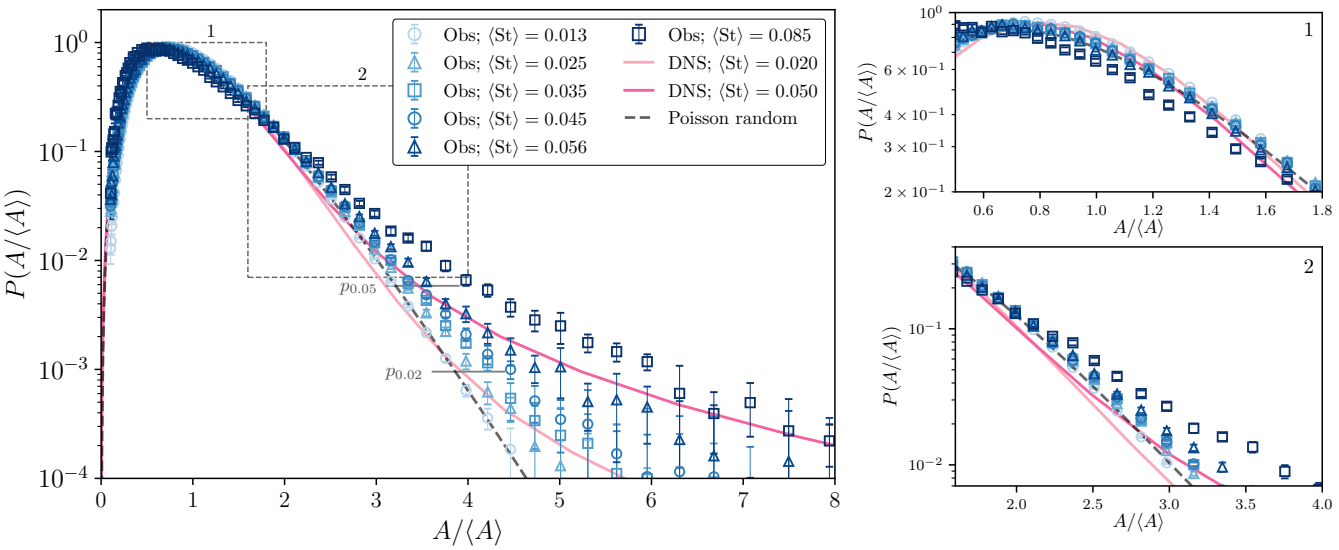

FIG. 3: PDF of the area of Voronoi cells from observations (symbols) and from DNS at $R_\lambda = 170$. The values of $\langle \mathrm{St}\rangle$ are indicated in the legend. The dashed line corresponds to the PDF of Voronoi areas for a set of random points [24–26]. The two pale horizontal lines correspond to probability, p_{St}, such that the distribution of $A/\langle A\rangle$ in the DNS differ, at the given value St by $\sim 8\%$ from the random distribution.

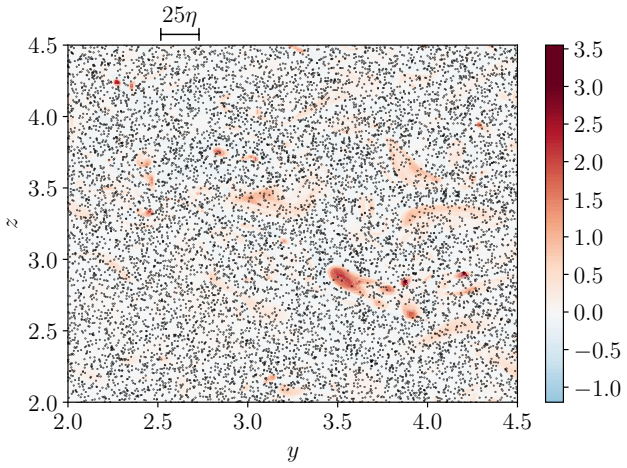

FIG. 4: Voids in the spatial distribution of particles in a direct numerical simulation of a turbulent flow at moderate Reynolds number ($R_\lambda = 170$), and St = 0.02, Sv = 0. Shown are particle positions (black dots) in a thin slice of the three-dimensional configuration space. The highly depleted regions of the flow correspond to large values of the the integral (3), indicated in red, see the color bars.

These features invalidate the expectation that $\mathcal{I}$ is necessarily small when St ~ 0.01, although the most intense vortex tubes are not the main reason why voids form.

To study the relation between void formation and the value of the integral $\mathcal{I}_T$ in a turbulent flow, we performed DNS of homogeneous isotropic turbulence by solving the Navier-Stokes equations at moderate Reynolds with the code GHOST [31]. The simulations were run at moderate resolution, up to 1024^3 grid points, and covered a range of values of the Taylor-scale based Reynolds number [32] up to $R_\lambda \sim 200$. This is much smaller than in cloud measurements (Fig. 2), where $\mathrm{Re}_\lambda \lesssim 10^3$, but sufficient to analyze void at small St. Starting with a large number of inertial particles, at $St \approx 0.02$, our visualization of the particle distribution reveals the existence of regions of low particle density, as shown in Fig. 4. The characteristic scale of these voids is $\sim 25\eta_K$, generally consistent with the observations in clouds,shown in Fig. 2. To characterize more precisely the statistics of voids, Fig. 3 shows the PDF of the areas of Voronoi cells throughout all the flow. The results suggest that one observes cells larger than expected from a random distribution of points with a probability of order $\sim 10^{-4}$ for St = 0.02 (blue curve). On the other hand, the distribution of size of Voronoi areas for St = 0.05 (red line) is very close to the corresponding distribution for experimental data at St = 0.047. Overall, there is a full consistency between the experimental and the numerical results, strongly suggesting that the origin of the voids can be attritbuted to the expulsion of weakly inertial droplets from vorticies in the flow.

One of the remarkable aspects is that the formation of voids depends very sensitively on St for values of the order of St $\gtrsim 10^{-2}$. Even for the value St = 0.02, it is important to notice that the most intense events in the flow, with a vorticity 10 times larger than the *rms* of vorticity fluctuations, is less than 10^{-6}. This leads to the

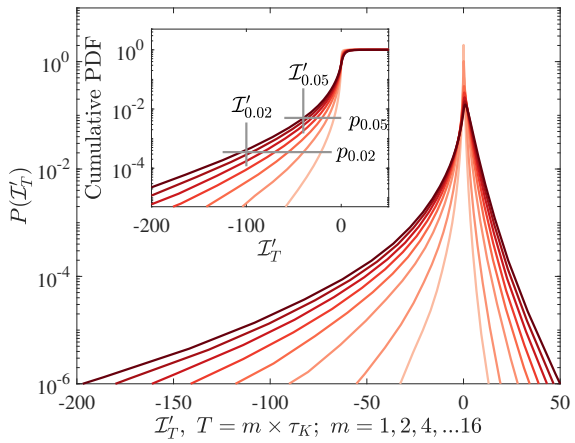

FIG. 5: PDF of the integral $\mathcal{I}'_T$, defined by Eq. (3). The PDFs are shown at values of T/τ_K equal to 1, and $2 \times n$ for $1 \leq n \leq 8$. As T increases, strong negative values of $\mathcal{I}'_T$ become more probable, although the distribution tends to saturate at large times. The inset shows the cumulative PDF for $T/\tau_K = 2 \times n$, for $1 \leq n \leq 16$. The Reynolds number of the flow is $R_\lambda = 170$. Along with the two probabilities $p_{\rm St}$ identified in Fig. 3, the two pale vertical lines correspond to $\mathcal{I}'_{\rm St} = -2/{\rm St}$, for which the integral in Eq. (3) is equal to -2.

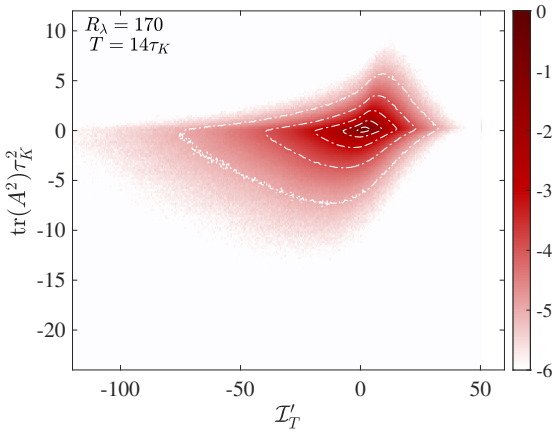

FIG. 6: Joint PDF of $-\mathcal{I}'_T\tau_K$ at $T = 14\tau_K$ (horizontal) $\mathrm{tr}(\mathbb{A}^2)\tau_K^2$ (horizontal). A strong value of the integral $-\mathcal{I}'_T$, necessary to form a void, does not correlate very strongly with regions of intense vorticity, which correpond to negative values of Q. The Reynolds number of the flow is $R_\lambda = 170$.

conclusion that the voids are not formed by the intense vortices in the flow, such that $\omega^2\tau_p^2 \approx 1$, as those vortices are much rarer than voids at the values of St considered. Fig. 5 shows the PDF of $\mathcal{I}'_T$ in a flow at $R_\lambda = 170$, as one follows the motion of tracers at times $T = 2n\tau_K$ for $1 \leq n \leq 7$, down to a probability $\sim 10^{-6}$. The figure shows a very dramatic growth of the negative tail as the time $T = n\tau_K$ increases. At short times, values of $\mathcal{I}'_T$ can reach values as large as ~ -50 with a probability $\gtrsim 10^{-4}$, reflecting the presence of very strong vortices – stronger vortices also exist in the flow, although with a much smaller probability. The positive side of the distribution of $\mathcal{I}'_T$ reflects strong fluctuations of the strain, $\mathrm{tr}\mathbb{S}^2$, which favor an increase in the density of heavy particles [6]. The growth of the positive tails is significantly more limited than that of the negative tails, which implies that the formation of regions of high density is limited. It is worth noting that for $T/\tau_K \gtrsim 14$, the distribution of $\mathcal{I}'_T$ does not change very much. We also compare the distribution of the Voronoi cell areas between the DNS and the experiments. We notice that the PDFs remain essentially constant when integrating the equations of motion forward in time, for a time $T \gtrsim 15\tau_K$. This time is of the order of $15\tau_K \sim 2.5\lambda_1^{-1}$, where λ_1 is the largest Lyapunov exponents for the tracer advection problem ($d\boldsymbol{x}/dt = \boldsymbol{u}$) [33]. In the following, we will keep a value of $T = 16\tau_K$.

The values of $\mathrm{St} \times \mathcal{I}'_T$ at the grid points are indicated by the color in Fig. 4. We observe that the regions with a low density of particles correlate with regions where $\mathrm{St} \times \mathcal{I}'_T$ is large, colored in red. In comparison, strong correlation of $\mathrm{St} \times \mathcal{I}'_T$ are very rare, and significantly less intense. Fig. 4 suggests that voids are associated with values of $\mathrm{St} \times \mathcal{I}'_T \lesssim 2$. In fact, we observe that the probability that $\mathrm{St} \times \mathcal{I}'_T$ is larger than ~ 2 is comparable to the probability of voids, as measured by the PDF of the area of Voronoi cells shown in Fig. 3.

We notice that the picture we are drawing does not explicitly rely on the most intense vortices at the location and time of the voids. The requirement for the integral $\mathcal{I}'_T$ to become large is that in the time interval $[-T, 0]$, the Lagrangian trajectory $\boldsymbol{x}(t)$ has experienced large fluctuations of the vorticity, sufficient to integrate to a very large value. As a consequence, the correlation between the integral $\mathcal{I}'_T(\boldsymbol{x})$ and the enstrophy, $|\omega|^2$, is not particularly strong, as soon as $T/\tau_K \gtrsim 5$, as revealed by Fig. 6 Again, we stress that very large values of $\omega_i\omega_i > 100\tau_K^{-2}$, which occur with a probability $\lesssim 10^{-8}$, cannot explain the formation of the voids observed with a much higher probability.

We have associated the observation of voids for values of St as small as $\mathrm{St} \approx 0.02$ to the distribution of the integral $\mathcal{I}_T$, which can reach very negative values, ensuring that particles can be expelled from regions of the flow. In comparison, large values of $\mathcal{I}'_T$ can also form, up to $\mathcal{I}'_T \approx 50$, see Fig. 5. The resulting values of $\mathcal{I}_T \equiv \mathrm{St}\mathcal{I}'_T$ are much of the order of $\approx 50\mathrm{St}$, suggests a significant increase of the density $n(\boldsymbol{x}_T, T)$, as predicted by Eq. (3). In fact, our analysis of the pair correlation function, in the spirit of [12], reveals clustering in the regions where $\mathcal{I}_T$ is appreciable. This aspect, which will be the subject of a separate publication, indicates that our approach allows us to describe weak, but measurable inhomogeneities in

the distribution of particles transported by turbulence. In this letter, we have shown that the presence of strong vorticity fluctuations in a turbulent flow can explain the formation of heterogeneities in a suspension of weakly inertial particles, such as droplets in a cloud. In fact, our DNS results reproduce quantitatively the distribution of Voronoi areas observed in the flow, see Fig. 3, and in particular the dependence on the Stokes numbers of the particles. The formation of voids can be explained by approximating the velocity of inertial particles by the simplified expression introduced in [6], and keeping track of the expulsion experienced by particles as the flow evolves. Importantly, the voids observed in the simulation are not due to the most intense vortices in the flow, which are too rare, but rather by intermediate vortices which are persistent enough. The results also explain the strong dependence of the expulsion mechanism on the Stokes number of the particles. Thus, turbulence itself may induce heterogeneities of the distribution of small, very weakly inertial droplets in a cloud. The interplay between these effects and entrainment and mixing of outside air [13] remains to be more fully explored.

[1] T. Birnstiel, F. M., and A. Johansen, *Space Sci. Rev.* **205**, 41 (2016).

[2] M. L. Pöhlker, C. Pöhlker, O. O. Krüger, J.-D. Förster, T. Berkemeier, W. Elbert, J. Fröhlich-Nowoisky, U. Pöschl, G. Bagheri, E. Bodenschatz, J. A. Huffman, S. Scheithauer, and E. Mikhailov, *Rev. Mod. Phys.* **95**, 045001 (2023).

[3] R. A. Shaw, *Annu. Rev. Fluid Mech.* **35** (2003).

[4] G. Falkovich, A. Fouxon, and M. Stepanov, *Nature* **419** (2002).

[5] E. Bodenschatz, S. Malinowski, S. R. A., and S. F., *Science* **327** (2010).

[6] M. R. Maxey, *J. Fluid Mech.* **174**, 441 (1987).

[7] G. Falkovich and A. Pumir, *Phys. Fluids* **16**, L47 (2004).

[8] A. Pumir and M. Wilkinson, *Annu. Rev. Condens. Matter Phys.* **7** (2016).

[9] W. W. Grabowski and P. Vaillancourt, *J. Atmosph. Sci.* **56**, 1433 (1999).

[10] K. Karpińska, J. F. E. Bodenschatz, S. P. Malinowski, J. L. Nowak, S. Risius, T. Schmeissner, R. A. Shaw, H. Siebert, H. Xi, H. Xu, and E. Bodenschatz, *Atmos. Chem. Phys.* **19**, 4991 (2019).

[11] M. L. Larsen, R. A. Shaw, A. B. Kostinski, and S. Glienke, *Phys. Rev. Lett.* **121** (2018).

[12] B. Thiede, M. J. Larsen, F. Nordsiek, O. Schlenczek, E. Bodenschatz, and G. Bagheri, *submitted* (2025).

[13] J. M. Yeom, I. Helman, P. Prabhakaran, J. C. Anderson, F. Yang, R. A. Shaw, and W. Cantrell, *Proc. Nat. Acad. Sci.* **120**, 2307354120 (2023).

[14] T. Oujia, K. Matsuda, and K. Schneider, *J. Fluid Mech.* **905** (2020).

[15] J. Matsuda, K. Yoshimatsu, and K. Schneider, *Phys. Rev. Lett.* **132** (2024).

[16] S. Sumbekova, A. Cartellier, A. Aliseda, and M. Bourgoin, *Physical Review Fluids* **2**, 024302 (2017).

[17] A. J. Petersen, L. Baker, and F. Coletti, *Journal of Fluid Mechanics* **864**, 925 (2019).

[18] R. Monchaux, M. Bourgoin, and A. Cartellier, *Physics of Fluids* **22**, 103304 (2010).

[19] E. W. Saw, R. A. Shaw, S. Ayyalasomayajula, P. Y. Chuang, and A. Gylfason, *Physical review letters* **100**, 214501 (2008).

[20] H. Yoshimoto and S. Goto, *Journal of Fluid Mechanics* **577**, 275 (2007).

[21] L. Baker, A. Frankel, A. Mani, and F. Coletti, *Journal of Fluid Mechanics* **833**, 364 (2017).

[22] P. J. Ireland, A. D. Bragg, and L. R. Collins, *Journal of Fluid Mechanics* **796**, 617 (2016).

[23] B. Stevens, S. Bony, D. Farrell, F. Ament, A. Blyth, C. Fairall, J. Karstensen, P. K. Quinn, S. Speich, C. Acquistapace, F. Aemisegger, A. L. Albright, H. Bellenger, E. Bodenschatz, K.-A. Caesar, R. Chewitt-Lucas, G. de Boer, J. Delanoë, L. Denby, F. Ewald, B. Fildier, M. Forde, G. George, S. Gross, M. Hagen, A. Hausold, K. J. Heywood, L. Hirsch, M. Jacob, F. Jansen, S. Kinne, D. Klocke, T. Kölling, H. Konow, M. Lothon, W. Mohr, A. K. Naumann, L. Nuijens, L. Olivier, R. Pincus, M. Pöhlker, G. Reverdin, G. Roberts, S. Schnitt, H. Schulz, A. P. Siebesma, C. C. Stephan, P. Sullivan, L. Touzé-Peiffer, J. Vial, R. Vogel, P. Zuidema, N. Alexander, L. Alves, S. Arixi, H. Asmath, G. Bagheri, K. Baier, A. Bailey, D. Baranowski, A. Baron, S. Barrau, P. A. Barrett, F. Batier, A. Behrendt, A. Bendinger, F. Beucher, S. Bigorre, E. Blades, P. Blossey, O. Bock, S. Böing, P. Bosser, D. Bourras, P. Bouruet-Aubertot, K. Bower, P. Branellec, H. Branger, M. Brennek, A. Brewer, P.-E. Brilouet, B. Brügmann, S. A. Buehler, E. Burke, R. Burton, R. Calmer, J.-C. Canonici, X. Carton, G. Cato Jr., J. A. Charles, P. Chazette, Y. Chen, M. T. Chilinski, T. Choularton, P. Chuang, S. Clarke, H. Coe, C. Cornet, P. Coutris, F. Couvreux, S. Crewell, T. Cronin, Z. Cui, Y. Cuypers, A. Daley, G. M. Damerell, T. Dauhut, H. Deneke, J.-P. Desbios, S. Dörner, S. Donner, V. Douet, K. Drushka, M. Dütsch, A. Ehrlich, K. Emanuel, A. Emmanouilidis, J.-C. Etienne, S. Etienne-Leblanc, G. Faure, G. Feingold, L. Ferrero, A. Fix, C. Flamant, P. J. Flatau, G. R. Foltz, L. Forster, I. Furtuna, A. Gadian, J. Galewsky, M. Gallagher, P. Gallimore, C. Gaston, C. Gentemann, N. Geyskens, A. Giez, J. Gollop, I. Gouirand, C. Gourbeyre, D. de Graaf, G. E. de Groot, R. Grosz, J. Güttler, M. Gutleben, K. Hall, G. Harris, K. C. Helfer, D. Henze, C. Herbert, B. Holanda, A. Ibanez-Landeta, J. Intrieri, S. Iyer, F. Julien, H. Kalesse, J. Kazil, A. Kellman, A. T. Kidane, U. Kirchner, M. Klingebiel, M. Körner, L. A. Kremper, J. Kretzschmar, O. Krüger, W. Kumala, A. Kurz, P. L'Hégaret, M. Labaste, T. Lachlan-Cope, A. Laing, P. Landschützer, T. Lang, D. Lange, I. Lange, C. Laplace, G. Lavik, R. Laxenaire, C. Le Bihan, M. Leandro, N. Lefevre, M. Lena, D. Lenschow, Q. Li,

G. Lloyd, S. Los, N. Losi, O. Lovell, C. Luneau, P. Makuch, S. Malinowski, G. Manta, E. Marinou, N. Marsden, S. Masson, N. Maury, B. Mayer, M. Mayers-Als, C. Mazel, W. McGeary, J. C. McWilliams, M. Mech, M. Mehlmann, A. N. Meroni, T. Mieslinger, A. Minikin, P. Minnett, G. Möller, Y. Morfa Avalos, C. Muller, I. Musat, A. Napoli, A. Neuberger, C. Noisel, D. Noone, F. Nordsiek, J. L. Nowak, L. Oswald, D. J. Parker, C. Peck, R. Person, M. Philippi, A. Plueddemann, C. Pöhlker, V. Pörtge, U. Pöschl, L. Pologne, M. Posyniak, M. Prange, E. Quiñones Meléndez, J. Radtke, K. Ramage, J. Reimann, L. Renault, K. Reus, A. Reyes, J. Ribbe, M. Ringel, M. Ritschel, C. B. Rocha, N. Rochetin, J. Röttenbacher, C. Rollo, H. Royer, P. Sadoulet, L. Saffin, S. Sandiford, I. Sandu, M. Schäfer, V. Schemann, I. Schirmacher, O. Schlenczek, J. Schmidt, M. Schröder, A. Schwarzenboeck, A. Sealy, C. J. Senff, I. Serikov, S. Shohan, E. Siddle, A. Smirnov, F. Späth, B. Spooner, M. K. Stolla, W. Szkółka, S. P. de Szoeke, S. Tarot, E. Tetoni, E. Thompson, J. Thomson, L. Tomassini, J. Totems, A. A. Ubele, L. Villiger, J. von Arx, T. Wagner, A. Walther, B. Webber, M. Wendisch, S. Whitehall, A. Wiltshire, A. A. Wing, M. Wirth, J. Wiskandt, K. Wolf, L. Worbes, E. Wright, V. Wulfmeyer, S. Young, C. Zhang, D. Zhang, F. Ziemen, T. Zinner, and M. Zöger, *Earth System Science Data* **13**, 4067 (2021).

[24] J.-S. Ferenc and Z. Neda, *Physica A: Statistical Mechanics and its Applications* **385**, 518 (2007).

[25] H. J. Hilhorst, *Journal of Statistical Mechanics: Theory and Experiment* **2009**, P05007 (2009).

[26] A. Gabrielli, *Journal of Statistical Mechanics: Theory and Experiment* **2009**, N07001 (2009).

[27] B. Stevens, S. Bony, D. Farrell, F. Ament, A. Blyth, et al., *Earth System Science Data* **13**, 4067 (2021).

[28] G. Haller and T. Sapsis, *Physica D* **573-583**, 254501 (2008).

[29] E. Balkovsky, G. Falkovich, and A. Fouxon, *Phys. Rev. Lett.* **86**, 2790 (2001).

[30] D. Buaria, A. Pumir, E. Bodenschatz, and P. K. Yeung, *New J. Physics* **21**, 043004 (2019).

[31] P. Mininni, D. Rosenberg, R. Reddy, and A. Pouquet, *Parallel Comput.* **37** (2011).

[32] S. B. Pope, *Turbulent flows*, 2000.

[33] P. L. Johnson and C. Meneveau, *Physics of Fluids* **27**, 085110 (2015).